
Whitening and second order optimization both destroy information about the dataset, and can make generalization impossible

Neha S. Wadia

University of California, Berkeley
neha.wadia@berkeley.edu

Daniel Duckworth

Google Brain
duckworthd@google.com

Samuel S. Schoenholz

Google Brain
schsam@google.com

Ethan Dyer

Google Brain
edyer@google.com

Jascha Sohl-Dickstein

Google Brain
jaschasd@google.com

Abstract

Machine learning is predicated on the concept of generalization: a model achieving low error on a sufficiently large training set should also perform well on novel samples from the same distribution. We show that both data whitening and second order optimization can harm or entirely prevent generalization. In general, model training harnesses information contained in the sample-sample second moment matrix of a dataset. We prove that for models with a fully connected first layer, the information contained in this matrix is the *only information* which can be used to generalize. Models trained using whitened data, or with certain second order optimization schemes, have less access to this information; in the high dimensional regime they have no access at all, producing models that generalize poorly or not at all. We experimentally verify these predictions for several architectures, and further demonstrate that generalization continues to be harmed even when theoretical requirements are relaxed. However, we also show experimentally that *regularized* second order optimization can provide a practical tradeoff, where training is still accelerated but less information is lost, and generalization can in some circumstances even improve.

1 Introduction

Whitening is a data preprocessing step that removes correlations between input features (see Fig. 1). It is widely used across many scientific disciplines, including geology [1], physics [2], machine learning [3], linguistics [4], and chemistry [5]. It has a particularly rich history in neuroscience, where it has been proposed as a mechanism by which biological neural networks realize Barlow’s redundancy reduction hypothesis [6–10].

Whitening is often recommended since, by standardizing the variances in each direction in feature space, it typically speeds up the convergence of learning algorithms [3, 11], and causes models to better capture contributions from low variance feature directions. Whitening can also encourage models to focus on more fundamental higher order statistics in data, by removing second order statistics [12]. Whitening has further been a direct inspiration for deep learning techniques such as batch normalization [13] and dynamical isometry [14, 15].

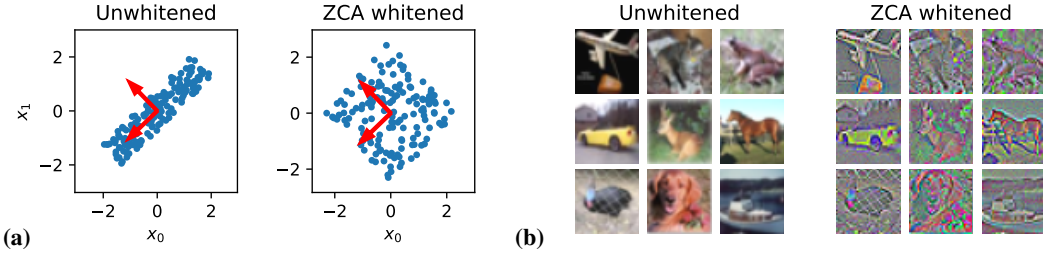


Figure 1: **Whitening removes correlations between feature dimensions in a dataset.** Whitening is a linear transformation of a dataset that sets all non-zero eigenvalues of the covariance matrix to 1. ZCA whitening is a specific choice of the linear transformation that rescales the data in the directions given by the eigenvectors of the covariance matrix, but without additional rotations or flips. (a) A toy 2d dataset before and after ZCA whitening. Red arrows indicate the eigenvectors of the covariance matrix of the unwhitened data. (b) ZCA whitening of CIFAR10 images preserves spatial and chromatic structure, while equalizing the variance across all feature directions.

1.1 Whitening destroys information useful for generalization

In the high dimensional setting, for any model with a fully connected first layer, we show theoretically and experimentally that whitening the data and then training with gradient descent or stochastic gradient descent (SGD) results in a model with poor or nonexistent generalization ability, depending on how the whitening transform is computed. Here, the high dimensional setting corresponds to a number of input features which is comparable to or larger than the number of datapoints. This setting is of particular relevance in fields where data collection is expensive or otherwise prohibitive [16], or where the data is intrinsically high dimensional [17–21], and is also the focus of increasing interest in statistics [22].

The loss of generalization ability for high dimensional whitened datasets is due to the fact that whitening destroys information in the dataset, and that *in high dimensional datasets whitening destroys all information which can be used for prediction*. This result is not restricted to neural networks, and applies to any model in which the input is transformed by a dense matrix multiply with isotropic weight initialization.

1.2 Second order optimization harms generalization similarly to whitening

Second order optimization algorithms take advantage of information about the curvature of the loss landscape to take a more direct route to a minimum [23, 24]. There are many approaches to second order or quasi-second order optimization [25–58], and there is active debate over whether second order optimization harms generalization [59–63]. The measure of curvature used in these algorithms is often related to feature-feature covariance matrices of the input, and of intermediate activations [25]. In some situations, it is already known that second order optimization is equivalent to steepest descent training on whitened data [64, 25].

The similarities between whitening and second order optimization allow us to argue that pure second order optimization also prevents information about the input distribution from being leveraged during training, and can harm generalization. We confirm this experimentally in Fig. 4. We do find, however, that when strongly regularized and carefully tuned, second order methods can lead to superior performance (Fig. 5).

2 Theory of whitening, second order optimization, and generalization

Consider a dataset $X \in \mathbb{R}^{d \times n}$ consisting of n independent d -dimensional examples. We adopt the notation F for the feature-feature second moment matrix and K for the sample-sample second moment matrix:

$$F = XX^\top \in \mathbb{R}^{d \times d}, \quad K = X^\top X \in \mathbb{R}^{n \times n}. \quad (1)$$

We assume that at least one of F or K is full rank. We omit normalization factors of $1/n$ and $1/d$ in the definitions of F and K , respectively, for notational simplicity in later sections.

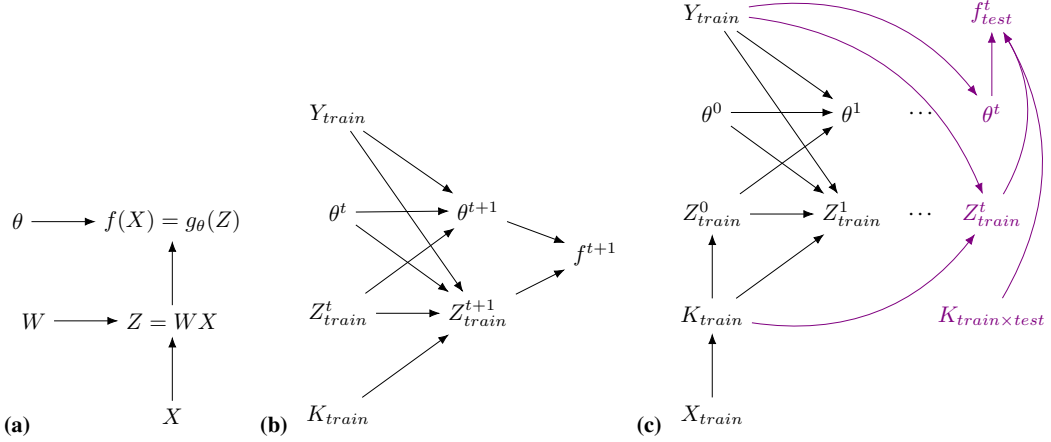


Figure 2: **Activations and weights depend on the training data only through second moments.** (a) Our model class consists of a linear transformation $Z = WX$, followed by a nonlinear map $g_\theta(Z)$ with parameters θ . (b) Causal dependencies for a single gradient descent update. The changes in weights, activations, and model output depend on the training data through the training sample second moment matrix, K_{train} , and the targets, Y_{train} . (c) Causal structure for the entire training trajectory. The final weights and training activations only depend on the training data through the training sample second moment matrix K_{train} , and the targets Y_{train} , while the test predictions (in purple) also depend on the mixed second moment matrix, $K_{train \times test}$.

Definition 2.0.1 (Whitening). *Any linear transformation M s.t. $\hat{X} = MX$ maps the eigenspectrum of F to ones and zeros, with the multiplicity of ones given by $\text{rank}(F)$.*

We consider the two cases $n \leq d$ and $n \geq d$ (when $n = d$ both cases apply).

$$\begin{aligned} n \geq d : \hat{F} &= I^{d \times d}, \quad \hat{K} = \sum_{i=1}^d \hat{u}_i \hat{u}_i^\top. \\ n \leq d : \hat{F} &= \sum_{j=1}^n \hat{v}_j \hat{v}_j^\top, \quad \hat{K} = I^{n \times n}. \end{aligned} \quad (2)$$

Here, \hat{F} and \hat{K} denote the whitened second moment matrices, and the vectors \hat{u}_i and \hat{v}_j are orthogonal unit vectors of dimension n and d respectively. Eq. 2 follows directly from the fact that $X^\top X$ and XX^\top share nonzero eigenvalues.

We are interested in understanding the effect of whitening on the performance of a trained model when evaluated on a test set. We will see that for models with a linear first layer, the trained model depends on the training data only through K . In general, training dynamics and generalization performance can depend non-trivially on K . However, whitening trivializes K , and so eliminates the ability of the network and training algorithm to take advantage of information contained in it.

2.1 Training dynamics depend on the training data only through its second moments

Consider a model f with a linear first layer Z :

$$f(X) = g_\theta(Z), \quad Z = WX, \quad (3)$$

where W denotes the first layer weights and θ denotes all remaining parameters (see Fig. 2(a)). W is initialized from an isotropic distribution. We study a supervised learning problem, in which each vector X_i corresponds to a label Y_i .¹ We adopt the notation $X_{train} \in \mathbb{R}^{d \times n_{train}}$ and Y_{train} for the training inputs and labels, and write the corresponding second moment matrices as F_{train} and K_{train} . We consider models with loss $L(f(X); Y)$ trained by SGD. The update rules are

$$\theta^{t+1} = \theta^t - \eta \frac{\partial L^t}{\partial \theta^t} \quad \text{and} \quad W^{t+1} = W^t - \eta \frac{\partial L^t}{\partial W^t} = W^t - \eta \frac{\partial L^t}{\partial Z_{train}^t} X_{train}^\top, \quad (4)$$

¹Our results also apply to unsupervised learning, which can be viewed as a special case of supervised learning where Y_i contains no information.

where t denotes the current training step, η is the learning rate, and L^t is the loss evaluated only on the minibatch used at step t .

As a result, the activations Z_{train} evolve as

$$Z_{\text{train}}^{t+1} = Z_{\text{train}}^t - \eta \frac{\partial L^t}{\partial Z_{\text{train}}^t} X_{\text{train}}^\top X_{\text{train}} = Z_{\text{train}}^t - \eta \frac{\partial L^t}{\partial Z_{\text{train}}^t} K_{\text{train}}. \quad (5)$$

Treating the weights, activations, and function predictions as random variables, with distributions induced by the initial distribution over W^0 , the update rules (Eqs. 4-5) can be represented by the causal diagram in Fig. 2(b). We can now state one of our main results.

Theorem 2.1.1. *Let $f(X)$ be a function as in Eq. 3, with linear first layer $Z = WX$, and additional parameters θ . Let W be initialized from an isotropic distribution. Further, let $f(X)$ be trained via gradient descent on a training dataset X_{train} . The learned weights θ^t and first layer activations Z_{train}^t are independent of X_{train} conditioned on K_{train} . In terms of mutual information \mathcal{I} , we have*

$$\mathcal{I}(Z_{\text{train}}^t, \theta^t; X_{\text{train}} \mid K_{\text{train}}, Y_{\text{train}}) = 0 \quad \forall t. \quad (6)$$

Proof. To establish this result, we note that the first layer activation at initialization, Z_{train}^0 , is a random variable due to random weight initialization, and only depends on X_{train} through K_{train} :

$$\mathcal{I}(Z_{\text{train}}^0; X_{\text{train}} \mid K_{\text{train}}) = 0. \quad (7)$$

This is a consequence of the isotropy of the initial weight distribution, explained in detail in Appendix A. Combining this with Eqs. 4-5, the causal diagram for all of training is given by (the black part of) Fig. 2(c). The conditional independence of Eq. 6 follows from this diagram. \square

2.2 Test set predictions depend on train and test inputs only through their second moments

Let $X_{\text{test}} \in \mathbb{R}^{d \times n_{\text{test}}}$ and Y_{test} be the test data. The test predictions $f_{\text{test}} = f(X_{\text{test}})$ are determined by $Z_{\text{test}}^t = W^t X_{\text{test}}$ and θ^t . So far we have discussed the evolution of Z_{train} . We can write the evolution of Z_{test} in a similar fashion:

$$Z_{\text{test}}^{t+1} = Z_{\text{test}}^t - \eta \frac{\partial L^t}{\partial Z_{\text{test}}^t} K_{\text{train} \times \text{test}}, \quad (8)$$

where $K_{\text{train} \times \text{test}} = X_{\text{train}}^\top X_{\text{test}} \in \mathbb{R}^{n_{\text{train}} \times n_{\text{test}}}$. The initial first layer activations are independent of the training data, and depend on X_{test} only through K_{test} :

$$\mathcal{I}(Z_{\text{test}}^0; X \mid K_{\text{test}}) = 0, \quad (9)$$

where X is the combined training and test data. If we denote the second moment matrix over this combined set by K , then the evolution of the test predictions is described by the (purple part of the) causal diagram in Fig. 2(c), from which we conclude the following.

Theorem 2.2.1. *For a function $f(X)$ as in Eq. 3, trained with the update rules Eqs. 4-5 from an isotropic weight initialization, test predictions depend on the training data only through K and Y_{train} . This is summarized in the mutual information statement*

$$\mathcal{I}(f_{\text{test}}; X \mid K, Y_{\text{train}}) = 0. \quad (10)$$

2.3 Whitening harms generalization

Full data whitening of a high dimensional dataset. We first consider a simplified setup: computing the whitening transform using the combined training and test data. We refer to this as ‘full-whitening’. We consider the large feature count ($d \geq n$) regime. In this case, by Eq. 2 we have $K = I$. Since K is now a constant rather than a stochastic variable, Eq. 10 reduces to

$$\mathcal{I}(f_{\text{test}}; \hat{X} \mid Y_{\text{train}}) = 0. \quad (11)$$

That is, *test set predictions contain no information about the model inputs X .* Model accuracy in this regime can be no higher than chance.

Training data whitening of a high dimensional dataset. In practice, we are more interested in the common setting of computing a whitening transform based only on the training data. We call data whitened in this way ‘train-whitened’. As mentioned above, the test predictions of a model are entirely determined by the first layer activations Z_{test}^t and the weights θ^t . From Theorem 2.1.1 we see that the learned weights θ^t depend on the training data only through K_{train} , and are thus independent of the training data for whitened data:

$$\mathcal{I}(\theta^t; \hat{X}_{\text{train}} \mid Y_{\text{train}}) = 0. \quad (12)$$

It is worth emphasizing this point because in most realistic networks the majority of model parameters are contained in these deeper weights θ^t .

Despite the deep layer weights, θ^t , being unable to extract information from the training distribution, the model is not entirely incapable of generalizing to test inputs. This is because the test activations Z_{test} will interpolate between training examples, using the information in $\hat{K}_{\text{train} \times \text{test}}$. More precisely,

$$Z_{\text{test}}^t = Z_{\text{test}}^0 + (Z_{\text{train}}^t - Z_{\text{train}}^0) \hat{K}_{\text{train} \times \text{test}}. \quad (13)$$

This interpolation in Z is the *only* way in which structure in the inputs X_{train} can drive generalization. This should be contrasted with the case of full data whitening, discussed above, where $\hat{K}_{\text{train} \times \text{test}} = 0$. We therefore predict that when whitening is performed only on the training data, there will be some generalization, but it will be much more limited than can be achieved without whitening.

2.4 Whitening in linear models

Linear models $f = WX$ provide another perspective on why whitening is harmful, which we discuss briefly here. A detailed exposition is in Appendix B.

For this section only, consider the low dimensional case $d < n$, where the loss has a unique global optimum W^* . The model predictions at this optimum are invariant to whitening. However, the effect of whitening on training is apparent in the dynamics of W during training. We focus on the continuous-time picture because it is the clearest, but similar statements can be made for gradient descent. Recall that v_i are the eigenvectors of F_{train} . Denoting the corresponding eigenvalues by λ_i , the dynamics of W under gradient flow are given by the decomposition

$$W(t) = \sum_{i=1}^d v_i w_i(t), \quad w_i(t) = e^{-t\lambda_i} w_i(0) + (1 - e^{-t\lambda_i}) w_i^*. \quad (14)$$

Eq. 14 shows that larger principal components of the data are learned faster than smaller ones. Whitening destroys this hierarchy by setting $\lambda_i = 1 \forall i$. If, for example, the data has a simplicity bias (large principal components correspond to signal and small ones correspond to noise), whitening forces the learning algorithm to fit signal and noise directions simultaneously, which results in poorer generalization at finite times during training than would be observed without whitening.

2.5 Newton’s method is equivalent to training on whitened data for linear models and for wide neural networks

We now compare a Newton update step on unwhitened data with a gradient descent update step on whitened data in a linear least squares model.

The Newton update step uses the model’s Hessian H as a preconditioner for the gradient:

$$W_{\text{Newton}}^{t+1} = W_{\text{Newton}}^t - \eta H^{-1} \frac{\partial L^t}{\partial W^t}. \quad (15)$$

For a linear model with mean squared error (MSE) loss, the Hessian is equal to the second moment matrix F_{train} and the model output evolves as

$$f_{\text{Newton}}^{t+1}(X) = f_{\text{Newton}}^t(X) - \eta \frac{\partial L^t}{\partial f_{\text{Newton}}^t} X_{\text{train}}^\top F_{\text{train}}^{-1} X. \quad (16)$$

We can compare this with the evolution of a linear model $\hat{f}(X) = \hat{W}MX$ trained via gradient descent on whitened data $\hat{X} = MX$:

$$\hat{f}^{t+1}(X) = \hat{f}^t(X) - \eta \frac{\partial L^t}{\partial \hat{f}^t} X_{\text{train}}^\top M^\top MX = \hat{f}^t(X) - \eta \frac{\partial L^t}{\partial \hat{f}^t} X_{\text{train}}^\top F_{\text{train}}^{-1} X. \quad (17)$$

The last line follows from rewriting the whitening matrix as a unitary matrix R applied to the zero-phase components analysis (ZCA) whitening matrix, $F^{-1/2}$ [65]. Thus $M = RF^{-1/2}$.

Eqs. 16 and 17 give identical update rules. Thus if both functions are initialized to have the same output, Newton updates give the same predictions as gradient descent training on whitened data. Applying the argument in Section 2.1, we expect Newton’s method to produce linear models that generalize poorly.

Finally, many neural network architectures, including fully connected and convolutional architectures, behave as linear models in their parameters throughout training in the large width limit [66]. The large width limit occurs when the number of units or channels in intermediate layers of the network grows towards infinity. Because of this, *second order optimization harms wide neural networks in the same way it harms linear models* (see Appendix C).

3 Experiments

3.1 Model and task descriptions

We describe our basic experiment structure, and follow this with descriptions of the four types of models we studied and associated experimental variations. Detailed methods are in Appendix E.

The kernel of all our experiments is as follows: From a dataset, we draw a number of subsets, tiling a range of dataset sizes. Each subset is divided into train, test, and validation examples, and three copies are made, two of which are whitened. In one case the whitening transform is computed using only the training examples, and in the other using all the data. Note that the test set size must be reduced in order to run experiments on small datasets, since the test set is considered part of the dataset for full-whitening. Models are trained from random initialization on each of the three copies of the data using the same training algorithm and stopping criterion. Test errors and the number of training epochs are recorded and plotted as functions of dataset size.

Linear Model. We study CIFAR-10 classification learned by optimizing mean squared error loss, where the model outputs are a linear map between the 512-dimensional outputs of a four layer convolutional network at random initialization on CIFAR-10, and their 10-dimensional one-hot labels. This setup is in part motivated by analogy to training the last layer of a deep neural network. We solve the gradient flow equation for the time at which the MSE on the validation set is lowest, and report the test error at that time. The experiment was repeated using Newton’s method.

Multilayer perceptron. We study fully connected three-layer MLPs on MNIST and CIFAR-10 classification tasks. Training is accomplished using SGD with constant step size until the training accuracy reaches a fixed cutoff threshold, at which point test accuracy is measured.

Convolutional networks. Since our theoretical results on the effect of whitening apply only to models with a fully connected first layer, we test whether the same qualitative behavior is observed in CNNs. We chose the popular wide residual (WRN) architecture [67], trained on CIFAR-10. Training was performed using full batch gradient descent with a cosine learning rate schedule for a fixed number of epochs. Full batch training was used to remove experimental confounds from choosing minibatch sizes at different dataset sizes. A validation set was split from the CIFAR-10 training set. Test error corresponding to the parameter values with the lowest validation error was reported.

We also trained a smaller CNN (a ResNet-50 convolutional block followed by an average pooling layer and a dense linear layer) on unwhitened data with full batch gradient descent and with the Gauss-Newton method (with and without a scaled identity regularizer) to compare their respective generalization performances. A grid search was performed over learning rate, and step sizes were chosen using a backoff line search initialized at that learning rate. Test and training losses corresponding to the best achieved validation loss were reported. Note that this experiment is relatively large scale; because we perform full second order optimization to avoid confounds due to choosing a quasi-Newton approximation, iterations are cubic in the number of model parameters.

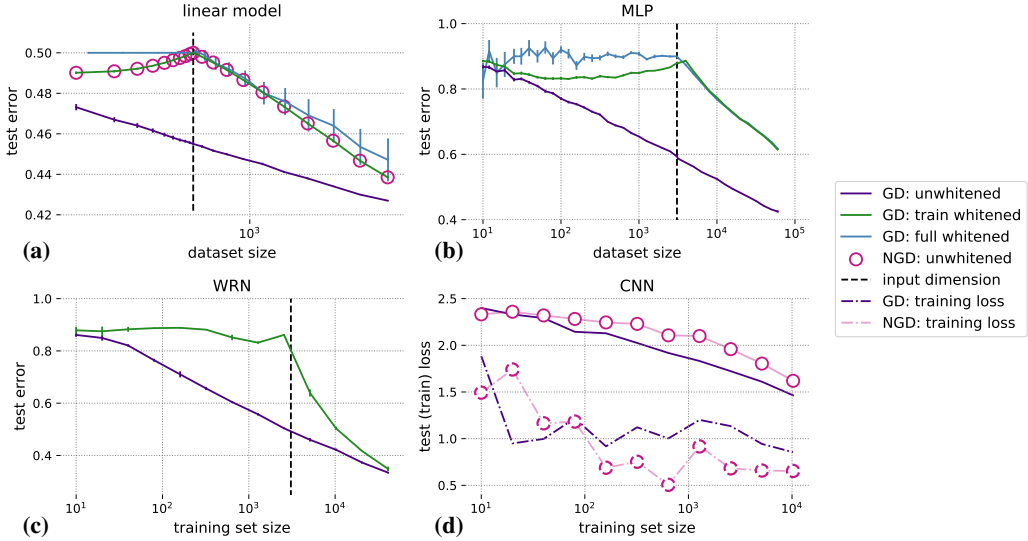


Figure 3: Whitening and second order optimization reduce or prevent generalization. (a)-(c) Models trained on both fully whitened data (blue; panes a,b) and train-whitened data (green; panes a-c) consistently underperform models trained by gradient descent on unwhitened data (purple; all panes). In (a), Newton’s method on unwhitened data (pink circles) behaves identically to gradient descent on whitened data. (d) Second order optimization in a convolutional network results in poorer generalization properties than steepest descent. Points plotted correspond to the learning rate and training step with the best validation loss for each method. Data for this experiment was unwhitened. CIFAR-10 is used for all experiments (see Appendix D for experiments on MNIST). In (c) and (d) we use a cross entropy loss (see Appendix E for details).

3.2 Experimental results

Whitening and second order optimization impair generalization. In agreement with theory, in Figs. 3(a) and (b), linear models and MLPs trained on fully whitened data generalize at chance levels (indicated by test errors of 0.5 and 0.9, respectively) until the size of the dataset exceeds the dimensionality of the data. After this point, generalization performance of the fully whitened model gradually recovers. Models trained on train-whitened data show reduced generalization ability, and perform strictly worse than models trained on unwhitened data. On CIFAR-10, a 20% gap in performance between MLPs trained on whitened and unwhitened data persists even at the largest dataset size. This suggests that whitening can remain detrimental even when the number of training examples exceeds the number of features by an order of magnitude.

The data in Fig. 3(c) indicates the presence of a generalization gap in the high dimensional regime between WRNs trained on train-whitened versus unwhitened data, despite the convolutional input layer violating the requirements of our theory. This gap persists as the size of the dataset grows beyond its input dimensionality. We note that these results are consistent with the whitening experiments in the original WRN paper [67]. Generalization ability begins to recover before the size of the training set reaches the input dimensionality of CIFAR-10, suggesting that the effect of whitening can be countered by engineering knowledge of the data statistics into the model architecture. Nonetheless, the presence of the generalization gap between whitened and unwhitened models at small and intermediate training set sizes reinforces the need to exercise caution when deciding whether or not to whiten data before training, even in architectures where our theoretical results do not directly apply.

In Fig. 3(a), the behavior of the test MSE of linear models trained on whitened data with gradient flow is identical to that of models trained on unwhitened data with Newton’s Method, demonstrating experimentally the correspondence we proved in Section 2.5. Second order optimization therefore equivalently harms generalization in this model. In Fig. 3(d), we observe a similar negative effect even in a convolutional network. Despite training to lower values of the training loss, a CNN trained with an unregularized Gauss-Newton method exhibits higher test loss (at the training step with best validation loss) than the same model trained with gradient descent.

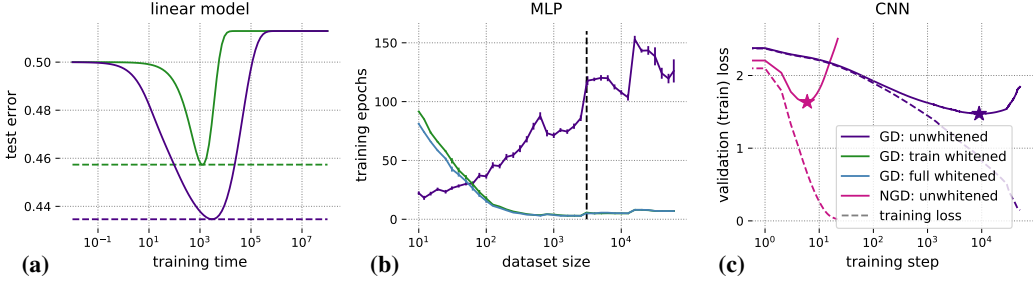


Figure 4: Models trained on whitened data or with second order optimizers converge faster. (a) Linear models trained on whitened data optimize faster, but their best test accuracy is always worse. Data plotted here is for a training set of size 2560. Similar results for smaller training set sizes are given in Fig. App.1. (b) Whitening the data significantly lowers the number of epochs needed to train an MLP, when the learning rate and all other training parameters are kept constant. (c) Second order optimization accelerates training on unwhitened data in a convolutional network, compared to gradient descent. Data shown is for a training set of size 10240. Stars correspond to values of the validation loss at which test and training losses are plotted in Fig. 3(d).

Whitening and second order optimization accelerate training Linear models trained on whitened data or with a second order optimizer converge to their final loss faster, though even for large dataset sizes their best test performance is worse than that of an unwhitened model. This is demonstrated in Fig. 4(a) for a single training set size of 2560 examples (similar results for smaller training sets are shown in Fig. App.1). MLPs trained on whitened CIFAR-10 data take fewer epochs to reach to the same training accuracy cutoff as MLPs trained on unwhitened data (Fig. 4(b)), except at very small (< 50) dataset sizes. The effect is stark at moderate and large dataset sizes, where models trained on whitened CIFAR-10 data require as little as two orders of magnitude fewer epochs to train. Discrete jumps in the plot data correspond to points at which the (constant) learning rate was changed (see Appendix E). Second order optimization similarly speeds up training in a convolutional network. In Fig. 4(c), unregularized Gauss-Newton descent achieves its best validation loss two orders of magnitude faster (as measured in the number of training steps) than gradient descent.

Regularized second order optimization can simultaneously accelerate training and improve generalization. In Fig. 5 we perform full batch second order optimization with a preconditioner of the form $((1 - \lambda)B + \lambda I)^{-1}$, where $\lambda \in [0, 1]$ is a regularization coefficient, and B^{-1} is the unregularized Gauss-Newton preconditioner. $\lambda = 0$ corresponds to unregularized Gauss-Newton, while $\lambda = 1$ corresponds to full batch steepest descent. At all values of $\lambda < 1$, regularized Gauss-Newton achieves its lowest validation loss in fewer training steps than steepest descent (Fig. 5(b)). For some values of λ , the regularized Gauss-Newton method additionally produces lower test loss values than steepest descent (Fig. 5(a)).

Regularized Gauss-Newton optimization acts similarly to unregularized Gauss-Newton in the subspace spanned by eigenvectors with eigenvalues larger than $\frac{\lambda}{1-\lambda}$, and similarly to steepest descent in the subspace spanned by eigenvectors with eigenvalues smaller than $\frac{\lambda}{1-\lambda}$. We therefore believe that regularized Gauss-Newton should be viewed as discarding information in the large-eigenvector subspace, though our theory does not formally address this case. We interpret the improved test performance with regularized Gauss-Newton in Fig. 5(a) as suggesting that this loss of information within the leading subspace is actually beneficial for the model on this dataset, likely due to aspects of the model’s inductive bias which are actively harmful on this task.

4 Discussion

Both theoretically and experimentally, we have shown that whitening data before training destroys information about the training distribution, and harms generalization. We have further shown that second order optimization can harm generalization in a similar fashion. Our results are strongest for the case that the input dimensionality exceeds the dataset size, but experimentally persist even when dataset size is increased far beyond this point.

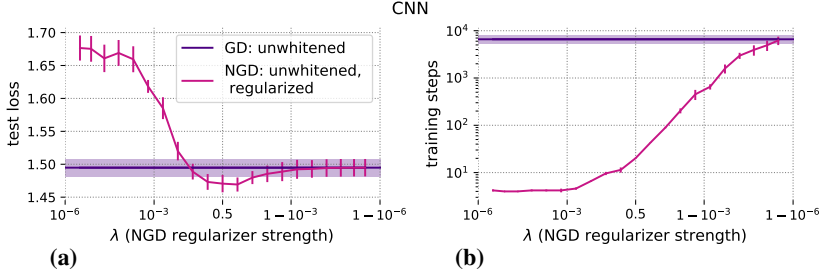


Figure 5: Regularized second order methods can train faster than gradient descent, with minimal or even positive impact on generalization. Models were trained on a size 10240 subset of CIFAR-10 by minimizing a cross entropy loss. Error bars indicate twice the standard error in the mean. (a) Test loss as a function of regularizer strength. At intermediate values of λ , the second order optimizer produces *lower* values of the test loss than gradient descent. Test loss is measured at the training step corresponding to the best validation performance for both algorithms. See text for further discussion. (b) At all values of $\lambda < 1$, the second order optimizer requires fewer training steps to achieve its best validation performance.

Are whitening and second order optimization a good idea? Our work suggests that both whitening and second order optimization come with costs – namely a likely reduction in the best achievable generalization. However, both whitening and second order optimization can drastically decrease training time – an effect we also see in our experiments. As available compute is typically a limiting factor on model performance [68], there are many scenarios where faster training may be worth the reduction in achievable generalization. Additionally, the negative effects on generalization may be largely resolved if the whitening transform or second order preconditioner are regularized, as is often done in practice [42]. We observe benefits from regularized second order optimization in Fig. 5, and similar results have been observed for whitening [69].

Directions for future work. The practice of whitening has, in the machine learning community, largely been replaced by batch normalization, for which it served as inspiration [13]. Studying connections between whitening and batch normalization, and especially understanding the degree to which batch normalization destroys information about the data distribution, may be particularly fruitful. Indeed, some results already exist in this direction [70].

Recent work analyzes deep neural networks through the lens of information theory [71–81], often computing measures of mutual information similar to those we discuss. Our result that the only usable information in a dataset is contained in its sample-sample second moment matrix K may inform or constrain this type of analysis.

Broader Impact

One of our perspectives on what whitening does and why it hurts generalization is that when data is whitened, different modes in the data that ordinarily have a hierarchy are put on equal footing, eliminating the distinction between signal and noise. In general, understanding how models implicitly or explicitly rely on different features is key to understanding and controlling what biases they develop. Not only does whitening put signal and noise on equal footing, but it removes hierarchies between features more generally. For example, whitening puts features that distinguish broad categories and minority categories on equal footing. In natural image classification, there is typically a hierarchy between when broad distinctions (e.g., animal vs. object) are learned and when fine grained distinctions (e.g., poodle vs. labradoodle) are learned. Whitening eliminates the hierarchy between these semantic categories. We believe that some of the insights of this work have the potential to help understand the interplay between the structure of data, optimization procedure, and biases that develop within neural networks.

More broadly, our work is directly relevant to researchers developing optimization algorithms, and to practitioners deciding how to preprocess their data and train their model. As such, it is multi-use, and may result in both positive and negative societal consequences. However, we believe that improving scientific understanding tends also to improve the human condition [82] – so in the absence of any

reason to expect harm, we believe that in expectation our work will have a positive impact on the world.

Acknowledgements

We thank Jeffrey Pennington for help formulating the project, and Justin Gilmer, Roger Grosse, Nicolas Le Roux, and Jesse Livezey for detailed feedback on a manuscript draft.

References

- [1] Alan R Gillespie, Anne B Kahle, and Richard E Walker. Color enhancement of highly correlated images. i. decorrelation and hsi contrast stretches. *Remote Sensing of Environment*, 20(3):209–235, 1986.
- [2] Fredrick A Jenet, George B Hobbs, KJ Lee, and Richard N Manchester. Detecting the stochastic gravitational wave background using pulsar timing. *The Astrophysical Journal Letters*, 625(2):L123, 2005.
- [3] Yann Le Cun, Léon Bottou, Genevieve B. Orr, and Klaus-Robert Müller. Efficient backprop. In *Neural Networks, Tricks of the Trade*, Lecture Notes in Computer Science LNCS 1524. Springer Verlag, 1998.
- [4] Steven Abney. *Semisupervised learning for computational linguistics*. Chapman and Hall/CRC, 2007.
- [5] Rasmus Bro and Age K Smilde. Principal component analysis. *Analytical Methods*, 6(9):2812–2831, 2014.
- [6] Fred Attneave. Some informational aspects of visual perception. *Psychol. Rev*, pages 183–193, 1954.
- [7] Horace Barlow. Possible principles underlying the transformations of sensory messages. *Sensory Communication*, 1, 01 1961.
- [8] Joseph J. Atick and A. Norman Redlich. What does the retina know about natural scenes? *Neural Comput.*, 4(2):196–210, March 1992.
- [9] Yang Dan, Joseph J. Atick, and R. Clay Reid. Efficient coding of natural scenes in the lateral geniculate nucleus: Experimental test of a computational theory. *Journal of Neuroscience*, 16(10):3351–3362, 1996.
- [10] Eero P Simoncelli and Bruno A Olshausen. Natural image statistics and neural representation. *Annual Review of Neuroscience*, 24(1):1193–1216, 2001.
- [11] Simon Wiesler and Hermann Ney. A convergence analysis of log-linear training. In *Proceedings of the 24th International Conference on Neural Information Processing Systems*, NIPS’11, pages 657–665, USA, 2011. Curran Associates Inc.
- [12] Aapo Hyvärinen, Jarmo Hurri, and Patrick O. Hoyer. *Natural Image Statistics: A Probabilistic Approach to Early Computational Vision*. Springer Publishing Company, Incorporated, 1st edition, 2009.
- [13] Sergey Ioffe and Christian Szegedy. Batch normalization: Accelerating deep network training by reducing internal covariate shift. In *Proceedings of the 32Nd International Conference on International Conference on Machine Learning - Volume 37*, ICML’15, pages 448–456. JMLR.org, 2015.
- [14] Jeffrey Pennington, Samuel Schoenholz, and Surya Ganguli. Resurrecting the sigmoid in deep learning through dynamical isometry: theory and practice. In *Advances in neural information processing systems*, pages 4785–4795, 2017.

[15] Lechao Xiao, Yasaman Bahri, Jascha Sohl-Dickstein, Samuel S Schoenholz, and Jeffrey Pennington. Dynamical isometry and a mean field theory of CNNs: How to train 10,000-layer vanilla convolutional neural networks. *arXiv preprint arXiv:1806.05393*, 2018.

[16] Hector J. Levesque, Ernest Davis, and Leora Morgenstern. The winograd schema challenge. In *13th International Conference on the Principles of Knowledge Representation and Reasoning, KR 2012*, pages 552–561, 2012.

[17] Carsen Stringer, Marius Pachitariu, Nicholas Steinmetz, Matteo Carandini, and Kenneth D. Harris. High-dimensional geometry of population responses in visual cortex. *Nature*, 571:361–365, 2019.

[18] Stefano Fusi, Earl K Miller, and Mattia Rigotti. Why neurons mix: high dimensionality for higher cognition. *Current Opinion in Neurobiology*, 37:66 – 74, 2016.

[19] Yu Shyr. Rigorous quantitative sciences integration – the foundation of high-dimensional genomic research. *Clinical and Experimental Metastasis*, 29:641–643, 2012.

[20] Manel Martínez-Ramón, Vladimir Koltchinskii, Gregory L. Heileman, and Stefan Posse. fMRI pattern classification using neuroanatomically constrained boosting. *NeuroImage*, 31(3):1129 – 1141, 2006.

[21] L. M. Bruce, C. H. Koger, and Jiang Li. Dimensionality reduction of hyperspectral data using discrete wavelet transform feature extraction. *IEEE Transactions on Geoscience and Remote Sensing*, 40(10):2331–2338, Oct 2002.

[22] Martin J. Wainwright. *High-Dimensional Statistics: A Non-Asymptotic Viewpoint*. Cambridge Series in Statistical and Probabilistic Mathematics. Cambridge University Press, 2019.

[23] Stephen Boyd and Lieven Vandenberghe. *Convex Optimization*. Cambridge University Press, USA, 2004. ISBN 0521833787.

[24] Léon Bottou, Frank E. Curtis, and Jorge Nocedal. Optimization methods for large-scale machine learning. *SIAM Review*, 60(2):223–311, 2018.

[25] James Martens and Roger Grosse. Optimizing neural networks with kronecker-factored approximate curvature. In *International conference on machine learning*, pages 2408–2417, 2015.

[26] John E Dennis Jr and Jorge J Moré. Quasi-Newton methods, motivation and theory. *SIAM review*, 19(1):46–89, 1977.

[27] CG Broyden. The convergence of a class of double-rank minimization algorithms 2. The new algorithm. *IMA Journal of Applied Mathematics*, 1970.

[28] R Fletcher. A new approach to variable metric algorithms. *The computer journal*, 1970.

[29] D Goldfarb. A family of variable-metric methods derived by variational means. *Mathematics of computation*, 1970.

[30] DF Shanno. Conditioning of quasi-Newton methods for function minimization. *Mathematics of computation*, 1970.

[31] Dong C DC Liu and Jorge Nocedal. On the limited memory BFGS method for large scale optimization. *Mathematical programming*, 45(1-3):503–528, 1989.

[32] Nicol Schraudolph, Jin Yu, and Simon Günter. A stochastic quasi-Newton method for online convex optimization. *AISTATS*, 2007.

[33] Peter Sunehag, Jochen Trumpf, S V N Vishwanathan, and Nicol Schraudolph. Variable metric stochastic approximation theory. *arXiv preprint arXiv:0908.3529*, August 2009.

[34] James Martens. Deep learning via Hessian-free optimization. In *Proceedings of the 27th International Conference on Machine Learning (ICML)*, volume 951, 2010.

[35] Richard H Byrd, Gillian M Chin, Will Neveitt, and Jorge Nocedal. On the use of stochastic hessian information in optimization methods for machine learning. *SIAM Journal on Optimization*, 21(3):977–995, 2011.

[36] Oriol Vinyals and Daniel Povey. Krylov subspace descent for deep learning. *arXiv preprint arXiv:1111.4259*, 2011.

[37] Chih-Jen Lin, Ruby C Weng, and S Sathiya Keerthi. Trust region newton method for logistic regression. *The Journal of Machine Learning Research*, 9:627–650, 2008.

[38] P Hennig. Fast probabilistic optimization from noisy gradients. *International Conference on Machine Learning*, 2013.

[39] RH Byrd, SL Hansen, J Nocedal, and Y Singer. A Stochastic Quasi-Newton Method for Large-Scale Optimization. *arXiv preprint arXiv:1401.7020*, 2014.

[40] Jascha Sohl-Dickstein, Ben Poole, and Surya Ganguli. Fast large-scale optimization by unifying stochastic gradient and quasi-newton methods. In *International Conference on Machine Learning*, pages 604–612, 2014.

[41] Guillaume Desjardins, Karen Simonyan, Razvan Pascanu, and koray kavukcuoglu. Natural neural networks. In C. Cortes, N. D. Lawrence, D. D. Lee, M. Sugiyama, and R. Garnett, editors, *Advances in Neural Information Processing Systems 28*, pages 2071–2079. Curran Associates, Inc., 2015.

[42] Roger Grosse and James Martens. A kronecker-factored approximate fisher matrix for convolution layers. *arXiv preprint arXiv:1602.01407*, 2016.

[43] James Martens, Jimmy Ba, and Matt Johnson. Kronecker-factored curvature approximations for recurrent neural networks. In *International Conference on Learning Representations*, 2018.

[44] Thomas George, César Laurent, Xavier Bouthillier, Nicolas Ballas, and Pascal Vincent. Fast approximate natural gradient descent in a kronecker-factored eigenbasis. In *Proceedings of the 32nd International Conference on Neural Information Processing Systems*, NIPS’18, page 9573–9583, Red Hook, NY, USA, 2018. Curran Associates Inc.

[45] Huishuai Zhang, Caiming Xiong, James Bradbury, and Richard Socher. Block-diagonal hessian-free optimization for training neural networks. *CoRR*, abs/1712.07296, 2017.

[46] Aleksandar Botev, Hippolyt Ritter, and David Barber. Practical gauss-newton optimisation for deep learning. In *Proceedings of the 34th International Conference on Machine Learning - Volume 70*, ICML’17, page 557–565. JMLR.org, 2017.

[47] Raghu Bollapragada, Jorge Nocedal, Dheevatsa Mudigere, Hao-Jun Shi, and Ping Tak Peter Tang. A progressive batching l-BFGS method for machine learning. In Jennifer Dy and Andreas Krause, editors, *Proceedings of the 35th International Conference on Machine Learning*, volume 80 of *Proceedings of Machine Learning Research*, pages 620–629, Stockholm Sweden, 10–15 Jul 2018. PMLR.

[48] Albert S. Berahas, Majid Jahani, and Martin Takáč. Quasi-newton methods for deep learning: Forget the past, just sample. *arXiv preprint arXiv:1901.09997*, 2019.

[49] Vineet Gupta, Tomer Koren, and Yoram Singer. Shampoo: Preconditioned stochastic tensor optimization. *CoRR*, abs/1802.09568, 2018.

[50] Naman Agarwal, Brian Bullins, and Elad Hazan. Second-order stochastic optimization for machine learning in linear time. *arXiv preprint arXiv:1602.03943*, 2016.

[51] John Duchi, Elad Hazan, and Yoram Singer. Adaptive subgradient methods for online learning and stochastic optimization. *Journal of Machine Learning Research*, 12(Jul):2121–2159, 2011.

[52] Noam Shazeer and Mitchell Stern. Adafactor: Adaptive learning rates with sublinear memory cost. *arXiv preprint arXiv:1804.04235*, 2018.

[53] Rohan Anil, Vineet Gupta, Tomer Koren, and Yoram Singer. Memory-efficient adaptive optimization for large-scale learning. *arXiv preprint arXiv:1901.11150*, 2019.

[54] Naman Agarwal, Brian Bullins, Xinyi Chen, Elad Hazan, Karan Singh, Cyril Zhang, and Yi Zhang. Efficient full-matrix adaptive regularization. In Kamalika Chaudhuri and Ruslan Salakhutdinov, editors, *Proceedings of the 36th International Conference on Machine Learning*, volume 97 of *Proceedings of Machine Learning Research*, pages 102–110, Long Beach, California, USA, 09–15 Jun 2019. PMLR.

[55] Yao Lu, Mehrtash Harandi, Richard I. Hartley, and Razvan Pascanu. Block mean approximation for efficient second order optimization. *ArXiv*, abs/1804.05484, 2018.

[56] Diederik P Kingma and Jimmy Ba. Adam: A method for stochastic optimization. *arXiv preprint arXiv:1412.6980*, 2014.

[57] Matthew D. Zeiler. ADADELTA: an adaptive learning rate method. *CoRR*, abs/1212.5701, 2012.

[58] T. Tieleman and G. Hinton. Lecture 6.5—RmsProp: Divide the gradient by a running average of its recent magnitude. COURSERA: Neural Networks for Machine Learning, 2012.

[59] Ashia C Wilson, Rebecca Roelofs, Mitchell Stern, Nati Srebro, and Benjamin Recht. The marginal value of adaptive gradient methods in machine learning. In *Advances in Neural Information Processing Systems*, pages 4148–4158, 2017.

[60] Guodong Zhang, Chaoqi Wang, Bowen Xu, and Roger Grosse. Three mechanisms of weight decay regularization. *arXiv preprint arXiv:1810.12281*, 2018.

[61] Guodong Zhang, James Martens, and Roger B Grosse. Fast convergence of natural gradient descent for over-parameterized neural networks. In H. Wallach, H. Larochelle, A. Beygelzimer, F. d’Alché-Buc, E. Fox, and R. Garnett, editors, *Advances in Neural Information Processing Systems 32*, pages 8082–8093. Curran Associates, Inc., 2019.

[62] Shun ichi Amari, Jimmy Ba, Roger Grosse, Xuechen Li, Atsushi Nitanda, Taiji Suzuki, Denny Wu, and Ji Xu. When does preconditioning help or hurt generalization?, 2020.

[63] Sharan Vaswani, Reza Babanezhad, Jose Gallego, Aaron Mishkin, Simon Lacoste-Julien, and Nicolas Le Roux. To each optimizer a norm, to each norm its generalization, 2020.

[64] Jascha Sohl-Dickstein. The natural gradient by analogy to signal whitening, and recipes and tricks for its use. *arXiv preprint arXiv:1205.1828*, 2012.

[65] Anthony J. Bell and Terrence J. Sejnowski. The “independent components” of natural scenes are edge filters. *Vision Research*, 37(23):3327 – 3338, 1997.

[66] Jaehoon Lee, Lechao Xiao, Samuel Schoenholz, Yasaman Bahri, Roman Novak, Jascha Sohl-Dickstein, and Jeffrey Pennington. Wide neural networks of any depth evolve as linear models under gradient descent. In *Advances in neural information processing systems*, pages 8570–8581, 2019.

[67] Sergey Zagoruyko and Nikos Komodakis. Wide residual networks. *CoRR*, abs/1605.07146, 2016.

[68] Christopher J Shallue, Jaehoon Lee, Joseph Antognini, Jascha Sohl-Dickstein, Roy Frostig, and George E Dahl. Measuring the effects of data parallelism on neural network training. *arXiv preprint arXiv:1811.03600*, 2018.

[69] Jaehoon Lee, Samuel S. Schoenholz, Jeffrey Pennington, Ben Adlam, Lechao Xiao, Roman Novak, and Jascha Sohl-Dickstein. Finite versus infinite neural networks:an empirical study. *in preparation*, 2020.

[70] Lei Huang, Dawei Yang, Bo Lang, and Jia Deng. Decorrelated batch normalization. *2018 IEEE/CVF Conference on Computer Vision and Pattern Recognition*, pages 791–800, 2018.

[71] Naftali Tishby and Noga Zaslavsky. Deep learning and the information bottleneck principle. In *2015 IEEE Information Theory Workshop (ITW)*, pages 1–5. IEEE, 2015.

[72] Raef Bassily, Shay Moran, Ido Nachum, Jonathan Shafer, and Amir Yehudayoff. Learners that use little information. *arXiv preprint arXiv:1710.05233*, 2017.

[73] Arindam Banerjee. On bayesian bounds. In *Proceedings of the 23rd international conference on Machine learning*, pages 81–88. ACM, 2006.

[74] Ravid Schwartz-Ziv and Naftali Tishby. Opening the black box of deep neural networks via information. *arXiv preprint arXiv:1703.00810*, 2017.

[75] A. Achille and S. Soatto. Emergence of Invariance and Disentangling in Deep Representations. *Proceedings of the ICML Workshop on Principled Approaches to Deep Learning*, 2017.

[76] Alessandro Achille and Stefano Soatto. Where is the information in a deep neural network? *arXiv preprint arXiv:1905.12213*, 2019.

[77] Rana Ali Amjad and Bernhard C Geiger. How (not) to train your neural network using the information bottleneck principle. *arXiv preprint arXiv:1802.09766*, 2018.

[78] Andrew M Saxe, Yamini Bansal, Joel Dapello, Madhu Advani, Artemy Kolchinsky, Brendan D Tracey, and David D Cox. On the information bottleneck theory of deep learning. *Journal of Statistical Mechanics: Theory and Experiment*, 2019(12):124020, Dec 2019.

[79] Artemy Kolchinsky, Brendan D Tracey, and Steven Van Kuyk. Caveats for information bottleneck in deterministic scenarios. *arXiv preprint arXiv:1808.07593*, 2018.

[80] Alexander A Alemi, Ian Fischer, Joshua V Dillon, and Kevin Murphy. Deep variational information bottleneck. *arXiv:1612.00410*, 2016.

[81] Ravid Schwartz-Ziv and Alexander A Alemi. Information in infinite ensembles of infinitely-wide neural networks. *arXiv preprint arXiv:1911.09189*, 2019.

[82] Steven Pinker. *Enlightenment now: The case for reason, science, humanism, and progress*. Penguin, 2018.

[83] Hanspeter Kraft and C. Procesi. Classical invariant theory: a primer. 1996.

[84] Andrew M. Saxe, James L. McClelland, and Surya Ganguli. Exact solutions to the nonlinear dynamics of learning in deep linear neural networks. In Yoshua Bengio and Yann LeCun, editors, *2nd International Conference on Learning Representations, ICLR 2014, Banff, AB, Canada, April 14-16, 2014, Conference Track Proceedings*, 2014.

[85] Nasim Rahaman, Aristide Baratin, Devansh Arpit, Felix Draxler, Min Lin, Fred A Hamprecht, Yoshua Bengio, and Aaron Courville. On the spectral bias of neural networks. *arXiv preprint arXiv:1806.08734*, 2018.

[86] Basri Ronen, David Jacobs, Yoni Kasten, and Shira Kritchman. The convergence rate of neural networks for learned functions of different frequencies. In H. Wallach, H. Larochelle, A. Beygelzimer, F. d’Alché-Buc, E. Fox, and R. Garnett, editors, *Advances in Neural Information Processing Systems 32*, pages 4761–4771. Curran Associates, Inc., 2019.

[87] Arthur Jacot, Franck Gabriel, and Clément Hongler. Neural tangent kernel: Convergence and generalization in neural networks. In *Advances in neural information processing systems*, pages 8571–8580, 2018.

[88] Ethan Dyer and Guy Gur-Ari. Asymptotics of wide networks from feynman diagrams. *ArXiv*, abs/1909.11304, 2020.

[89] Jiaoyang Huang and H B Yau. Dynamics of deep neural networks and neural tangent hierarchy. *ArXiv*, abs/1909.08156, 2019.

[90] Etaf Littwin, Tomer Galanti, and L. Wolf. On the optimization dynamics of wide hypernetworks. *ArXiv*, abs/2003.12193, 2020.

- [91] Anders Andreassen and Ethan Dyer. Asymptotics of wide convolutional neural networks. To appear.
- [92] Kyle Aitken and Guy Gur-Ari. On the asymptotics of wide networks with polynomial activations. To appear.

A Isotropy of weight initialization implies conditional independence

In this section we show that for isotropic initial weight distributions,

$$P(W^0 R) = P(W^0) \forall R \in O(d), \quad (18)$$

the training activations Z_{train} depend on the training data X_{train} only through the second moment matrix K_{train} . This is summarized in Eq. 7 repeated here for convenience:

$$\mathcal{I}(Z_{\text{train}}^0; X_{\text{train}} | K_{\text{train}}) = 0.$$

The argument is as follows, the isotropy of the weight distribution implies that the distribution of first layer activations conditioned on the training data is invariant under orthogonal transformations.

$$P(Z_{\text{train}}^0 | RX_{\text{train}}) = P(Z_{\text{train}}^0 | X_{\text{train}}) \forall R \in O(d). \quad (19)$$

To derive this we can write the distribution over Z_{train}^0 in terms of the distribution over initial weights, $P(Z_{\text{train}}^0 | X_{\text{train}}) = \int DW^0 P(W^0) \delta(Z_{\text{train}}^0 - W^0 X_{\text{train}})$. Here DW^0 is the uniform measure over the components of W^0 . We then have

$$\begin{aligned} P(Z_{\text{train}}^0 | RX_{\text{train}}) &= \int DW^0 P(W^0) \delta(Z_{\text{train}}^0 - W^0 RX_{\text{train}}) \\ &= \int D\tilde{W}^0 P(\tilde{W}^0 R^T) \delta(Z_{\text{train}}^0 - \tilde{W}^0 X_{\text{train}}) \\ &= \int D\tilde{W}^0 P(\tilde{W}^0) \delta(Z_{\text{train}}^0 - \tilde{W}^0 X_{\text{train}}) = P(Z_{\text{train}}^0 | X_{\text{train}}). \end{aligned} \quad (20)$$

To arrive at the second line we defined $\tilde{W}^0 := W^0 R$ and used the invariance of the measure DW^0 . The third line follows from the $O(d)$ invariance of the initial weight distribution. Now that we have established the rotational invariance of the distribution over first layer activations we can derive Eq. 7.

By the first fundamental theorem of invariant theory [83], the only $O(d)$ invariant functions of n vectors in d dimensions are the n^2 inner products $K_{\text{train}} = X_{\text{train}}^\top X_{\text{train}}$. Thus $P(Z_{\text{train}}^0 | X_{\text{train}}) = h(K_{\text{train}})$ for some function h , and $P(Z_{\text{train}}^0 | X_{\text{train}}, K_{\text{train}}) = P(Z_{\text{train}}^0 | K_{\text{train}})$. Eq. 7 then follows from the definition of conditional mutual information.

$$\begin{aligned} I(Z_{\text{train}}^0; X_{\text{train}} | K_{\text{train}}) &:= \mathbb{E}_{K_{\text{train}}} [D_{\text{KL}}(P(Z_{\text{train}}^0, X_{\text{train}} | K_{\text{train}}) || P(Z_{\text{train}}^0 | K_{\text{train}}) P(X_{\text{train}} | K_{\text{train}}))] \\ &= \mathbb{E}_{K_{\text{train}}} [P(X_{\text{train}} | K_{\text{train}}) D_{\text{KL}}(P(Z_{\text{train}}^0 | X_{\text{train}}, K_{\text{train}}) || P(Z_{\text{train}}^0 | K_{\text{train}}))] \\ &= 0. \end{aligned} \quad (21)$$

B Whitening in linear models

Linear models are widely used for regression and prediction tasks and provide an instructive laboratory to understand the effects of data whitening. Furthermore, linear models provide additional intuition for why whitening is harmful – whitening puts signal and noise directions in the data second moment matrix, F , on equal footing (see Fig. 1). For data with a good signal to noise ratio, unwhitened models learn high signal directions early during training and only overfit to noise at late times. For models trained on whitened data, the signal and noise directions are fit simultaneously and thus the models overfit immediately.

Consider a linear model with mean squared error loss,

$$f(X) = WX, \quad L = \frac{1}{2} \|f(X) - Y\|^2. \quad (22)$$

This loss function is convex. Here we focus on the low dimensional case, $d < n$, where the loss has a unique global optimum $W^* = F_{\text{train}}^{-1} X_{\text{train}} Y_{\text{train}}$. The model predictions at this global optimum, $f_*(X) = W^* X$, are invariant under any whitening transform (2.0.1). As a result, any quality metric (loss, accuracy, etc...) for this global minimum is the same for whitened and unwhitened data.

The story is more interesting, however, during training. Consider a model trained via gradient flow (similar statements can be made for gradient descent or stochastic gradient descent). The dynamics of the weights are given by

$$\frac{dW}{dt} = -\frac{\partial L}{\partial W}, \quad W(t) = e^{-tF_{\text{train}}} W(0) + (1 - e^{-tF_{\text{train}}}) W^*. \quad (23)$$

The evolution in Eq. 23 implies that the information contained in the trained weights $W(t)$ about the training data X is entirely determined by F and W^* . In terms of mutual information, we have

$$\mathcal{I}(W(t); X | F_{\text{train}}, W^*) = 0. \quad (24)$$

As whitening sets $\hat{F}_{\text{train}} = I$, a linear model trained on whitened data does not benefit from the information in F_{train} .

At a more microscopic level, we can decompose Eq. 23 in terms of the eigenvectors, v_i , of F :

$$W(t) = \sum_{i=1}^d v_i w_i(t), \quad w_i(t) = e^{-t\lambda_i} w_i(0) + (1 - e^{-t\lambda_i}) w_i^*. \quad (25)$$

We see that for unwhitened data the eigen-modes with larger eigenvalue converge more quickly towards the global optimum, while the small eigen-directions converge slowly. For centered X , F is the feature covariance and these eigen-directions are exactly the principle components of the data. As a result, training on unwhitened data is biased towards learning the top principal directions at early times. This bias is often beneficial for generalization. Similar simplicity biases have been found empirically in deep linear networks [84] and in deep networks trained via SGD [85, 86] where networks learn low frequency modes before high. In contrast, for whitened data, $\hat{F}_{\text{train}} = I$ and the evolution of the weights takes the form

$$\hat{w}_i(t) = e^{-t} \hat{w}_i(0) + (1 - e^{-t}) \hat{w}_i^*. \quad (26)$$

All hierarchy between the principle directions has been removed, thus training fits all directions at a similar rate. For this reason linear models trained on unwhitened data can generalize significantly better at finite times than the same models trained on whitened data. Empirical support for this in a linear image classification task with random features is shown in Fig. 3(a).

C Second order optimization of wide neural networks

Here we consider second order optimization for wide neural networks. In recent years much progress has been made in understanding the dynamics of wide neural networks [87], in particular it has been realized that wide networks trained via GD, SGD or gradient flow evolve as a linear model with static, nonlinear features given by the derivative of the network map at initialization [66].

In this section we extend the connection between linear models and wide networks to second order methods. In particular we argue that *wide networks trained via a regularized Newton's method evolve as linear models trained with the same second order optimizer*.

We consider a regularized Newton update step,

$$\theta^{t+1} = \theta^t - \eta (\epsilon \mathbf{1} + H)^{-1} \frac{\partial L^t}{\partial \theta}. \quad (27)$$

This diagonal regularization is a common generalization of Newton's method. One motivation for such an update rule in the case of very wide neural networks is that the Hessian is necessarily rank deficient, and so some form of regularization is needed.

For a linear model, $f_{\text{linear}}(x) = \theta^\top \cdot g(x)$, with fixed non-linear features, $g(x)$, the regularized newton update rule in weight space leads to the function space update.

$$f_{\text{linear}}^{t+1}(x) = f_{\text{linear}}^t(x) - \eta \sum_{x_a, x_b \in X_{\text{train}}} \Theta_{\text{linear}}(x, x_a) (\epsilon \mathbf{1} + \Theta_{\text{linear}})_{ab}^{-1} \frac{\partial L_b}{\partial f_{\text{linear}}}. \quad (28)$$

Here, Θ_{linear} , is a constant kernel, $\Theta_{\text{linear}}(x, x') = \frac{\partial f}{\partial \theta}^\top \cdot \frac{\partial f}{\partial \theta} = g^\top(x) \cdot g(x')$.

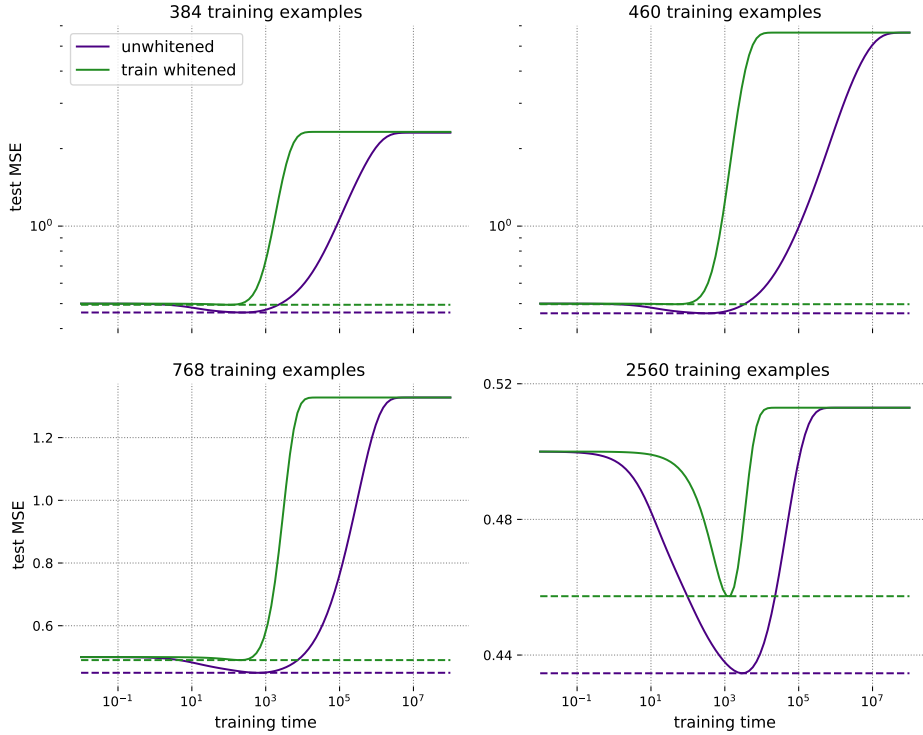


Figure App.1: **Whitening data speeds up training but reduces generalization in linear models.** Here we show representative examples of the evolution of test error with training time in a linear least-squares model where the training set consists of 384, 460, 768, 2560 examples, as labeled. In all cases, while models trained on train-whitened data (in green) reach their optimal mean squared errors in a smaller number of epochs, they do no better than models trained on unwhitened data (in purple). In the large time limit of training, the two kinds of models are indistinguishable as measured by test error. The y -axis in the top row of plots is in log scale for clarity.

For a deep neural network, the function space update takes the form.

$$\begin{aligned}
 f^{t+1}(x) = & f^t(x) - \eta \sum_{x_a, x_b \in X_{\text{train}}} \Theta(x, x_a) (\epsilon \mathbf{1} + \Theta)^{-1}_{ab} \frac{\partial L_b}{\partial f} \\
 & + \frac{\eta^2}{2} \sum_{\mu, \nu=1}^P \frac{\partial^2 f}{\partial \theta_\mu \partial \theta_\nu} \Delta \theta_\mu^t \Delta \theta_\nu^t + \dots
 \end{aligned} \tag{29}$$

Here we have indexed the model weights by $\mu = 1 \dots P$, denoted the change in weights by $\Delta \theta^t$ and introduced the neural tangent kernel (NTK), $\Theta(x, x') = \frac{\partial f^\top}{\partial \theta} \cdot \frac{\partial f}{\partial \theta}$.

In general Eqs. 28 and 29 lead to different network evolution due to the non-constancy of the NTK and the higher order terms in the learning rate. For wide neural networks, however, it was realized that the NTK is constant [87] and the higher order terms in η appearing on the second line in vanish at large width [88–92].²

With these simplifications, the large width limit of Eq. 29 describes the same evolution as a linear model trained with fixed features $g(x) = \frac{\partial f(x)}{\partial \theta}|_{\theta=\theta_0}$ trained via a regularized Newton update.

²These simplifications were originally derived for gradient flow, gradient descent and stochastic gradient descent, but hold equally well for the regularized Newton updates considered here. This can be seen, for example, by applying Theorem 1 of [88].

D MLP on MNIST

Here we present the equivalent of Fig. 3(b) for an MLP trained on MNIST. Experimental details are given in Appendix E. Similar to the results in Fig. 3(b) on CIFAR-10, in Fig. App.2, we find that models trained on fully whitened data generalize at chance levels (indicated by a test error of 0.9) in the high dimensional regime. Because MNIST is highly rank deficient, this result holds until the size of the dataset exceeds its input rank. Models trained on train-whitened data also exhibit reduced generalization when compared with models trained on unwhitened data, which exhibit steady improvement in generalization with increasing dataset size.

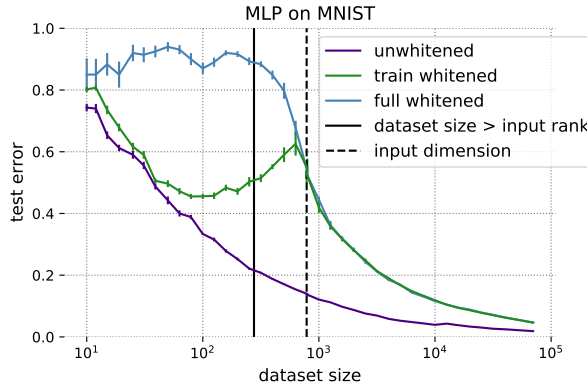


Figure App.2: **Whitening MNIST before training negatively impacts generalization in MLPs.** Models trained on fully whitened data (in blue) are unable to generalize until the size of the dataset exceeds its maximal input rank of 276, indicated by the solid black vertical line. Regardless of how the whitening transform is computed, models trained on whitened data (blue and green) consistently underperform those trained on unwhitened data (in purple).

E Methods

E.1 Whitening Methods

E.1.1 PCA Whitening

Consider a dataset $X \in \mathbb{R}^{d \times n}$. PCA whitening can be viewed as a two-step operation involving rotation of X into the PCA basis, followed by the normalization of all PCA components to unity. We implement this transformation as follows. First, we compute the the singular value decomposition of the unnormalized feature-feature second moment matrix XX^\top :

$$XX^\top = U\Sigma V^\top, \quad (30)$$

where the rank of Σ is $\min(n, d)$. The PCA whitening transform is then computed as $M = \Sigma^{-1/2} \cdot V^\top$, where the dot signifies element-wise multiplication between the whitening coefficients, $\Sigma^{-1/2}$, and their corresponding singular vectors. When Σ is rank deficient ($n < d$), we use one of two methods to stabilize the computation of the inverse square root: the addition of noise, or manual rank control. In the former, a small jitter is added to the diagonal elements of Σ before inverting it. This was implemented in the experiments in linear models. In the latter, the last $d - n$ diagonal elements of $\Sigma^{-1/2}$ are explicitly set to unity. This method was implemented in the MLP experiments.

E.1.2 ZCA Whitening

ZCA (short for zero-phase components analysis) [65] can be thought of as PCA whitening followed by a rotation back into the original basis. The ZCA whitening transform is $M = U\Sigma^{-1/2} \cdot V^\top$. ZCA whitening produces images that look like real images, preserving local structure. For this reason, it is used in the CNN experiments.

E.2 Linear Model

Dataset composition. The dataset for this experiment was a modified version of CIFAR-10, where the images were first processed by putting them through an off-the-shelf (untrained) four layer convolutional network with tanh nonlinearities and collecting the outputs of the penultimate layer. This resulted in a dataset of 512-dimensional images and their associated labels. Both the CIFAR-10 training and test sets were processed in this way. The linear estimator was trained to predict one-hot (ten dimensional) labels.

Training set sizes ranged from 128 to 5120 examples, randomly sampled from the preprocessed CIFAR-10 data. For experiments on unwhitened and train-whitened data, a validation set of 10000 images was split from the CIFAR-10 training set, and test error was measured on the CIFAR-10 test set. For experiments on fully whitened data, validation and test sets of 10 images each were split from the CIFAR-10 training and test sets, respectively.

Whitening. At each training set size, three copies of the data were made, and two were whitened using the PCA whitening method. For train-whitened data, the whitening transform was computed using only the training examples. For fully whitened data, the twenty validation and test images were included in the computation of the whitening transform.

Training and Measurements. We used a mean squared error loss function. At each training set size, fifty models (initialized with different random seeds) were trained with full-batch gradient descent, with the optimization path defined by the gradient flow equation. Writing the model parameters as ϕ , this equation is

$$\phi(t) = \phi^* + e^{-tCB}(\phi^* - \phi^{(0)})$$

for preconditioner B , feature-feature correlation matrix C , infinite-time solution θ^* , and initial iterate $\phi^{(0)}$. In the case of gradient descent, the preconditioner B is simply the identity matrix.

In order to generate the plot data for Fig. 3(a), we solved the gradient flow equation for the parameters ϕ that achieved the lowest validation error, and calculated the test error achieved by those parameters. Mean test errors and their inner 80th percentiles across the twenty different initializations and across whitening states were computed and plotted. To make the plots in Fig. 4(a) and App.1, we tracked test performance over the course of training on unwhitened and train-whitened data.

On train-whitened datasets, we also implemented Newton’s Method. This was done by putting the preconditioner B in the gradient flow equation equal to the inverse Hessian, i.e. $(XX^\top)^{-1}$. The preconditioner was computed once using the whole training set, and remained constant over the course of training. For experiments on whitened data, the data was whitened before computing the preconditioner.

E.3 Multilayer Perceptron

E.3.1 On MNIST

Architecture. We used a $784 \times 512 \times 512 \times 10$ fully connected network with a rectified linear nonlinearity in the hidden layers and a softmax function at the output layer. Initial weights were sampled from a normal distribution with variance 10^{-4} .

Dataset composition. The term “dataset size” here refers to the total size of the dataset, i.e. it counts the training as well as test examples. We did not use validation sets in the MLP experiments. Datasets of varying sizes were randomly sampled from the MNIST training and test sets. Dataset sizes were chosen to tile the available range (0 to 70000) evenly in log space. The smallest dataset size was 10 and the two largest were 50118 and 70000. For all but the largest size, the ratio of training to test examples was 8 : 2. The largest dataset size corresponded to the full MNIST dataset, with its training set of 60000 images and test set of 10000 images.

The only data preprocessing step (apart from whitening) that we performed was to normalize all pixel values to lie in the range $[0, 1]$.

Whitening. At each dataset size, three copies of the dataset were made and two were whitened. Of these, one was train-whitened and the other fully whitened. PCA whitening was performed. The same whitening transform was always applied to both the training and test sets.

Training and Measurements. We used sum of squares loss function. Training was performed with SGD using a constant learning rate and batch size, though these were both modulated according to dataset size. Between a minimum of 2 and a maximum of 200, batch size was chosen to be a hundredth of the number of training examples. We chose a learning rate of 0.1 if the number of training examples was ≤ 50 , 0.001 if the number of training examples was ≥ 10000 , and 0.01 otherwise. Models were trained to 0.999 training accuracy, at which point the test accuracy was measured, along with the number of training epochs, and the accuracy on the full MNIST test set of 10000 images. This procedure was repeated twenty times, using twenty different random seeds, for each dataset. Means and standard errors across random seeds were calculated and are plotted in Fig. App.2.

For example, at the smallest dataset size of 10, the workflow was as follows. Eight training images were drawn from the MNIST training and two as test images were drawn from the MNIST test set. From this dataset, two more datasets were constructed by whitening the images. In one case the whitening transform was computed using only the eight training examples, and in another by using all ten images. Three copies of the MLP were initialized and trained on the eight training examples of each of the three datasets to a training accuracy of 0.999. Once this training accuracy was achieved, the test accuracy of each model on the two test examples, and on the full MNIST test set, was recorded, along with the number of training epochs. This entire procedure was repeated twenty times.

Computation of the input rank of MNIST data. MNIST images are encoded by 784 pixel values. However, the input rank of MNIST is much smaller than this. To estimate the maximal input rank of MNIST, at each dataset size (call it n) we constructed twenty samples of n images from MNIST. For each sample, we computed the 784×784 feature-feature second moment matrix F and its singular value decomposition, and counted the number of singular values larger than some cutoff. The cutoff was 10^{-5} times the largest singular value of F for that sample. We averaged the resulting number, call it r , over the twenty samples. If $r = n$, we increased n and repeated the procedure, until we arrived at the smallest value of n where $r > n$, which was 276. This is what we call the maximal input rank of MNIST, and is indicated by the solid black line in the plot in Appendix D.

E.3.2 On CIFAR-10

The procedure for the CIFAR-10 experiments was almost identical to the MNIST experiments described above. The differences are given here.

The classifier was of shape $3072 \times 2000 \times 2000 \times 10$ - slightly larger in the hidden layers and of necessity in the input layer.

The learning rate schedule was as follows: 0.01 if the number of training examples was ≤ 504 , then dropped to 0.005 until the number of training examples exceeded 2008, then dropped to 0.001 until the number of training examples exceeded 10071, and 0.0005 thereafter.

The CIFAR-10 dataset is full rank in the sense that the input rank of any subset of the data is equal to the dimensionality, 3072, of the images.

E.3.3 Fig. 3(b), App.2 plot details

In Figs. 3(b) and App.2, for models trained on unwhitened data and train-whitened data, we have plotted test error evaluated on the full CIFAR-10 and MNIST test sets of 10000 images. For models trained on fully whitened data, we have plotted the errors on the test examples that were included in the computation of the whitening transform.

E.4 Convolutional Networks

E.4.1 WRN

Architecture. We use the ubiquitous Wide ResNet 28-10 architecture from [67]. This architecture starts with a convolutional embedding layer that applies a 3×3 convolution with 16 channels. This is followed by three “groups”, each with four residual blocks. Each residual block features two instances of a batch normalization layer, a convolution, and a ReLU activation. The three block groups feature convolutions of 160 channels, 320 channels, and 640 channels, respectively. Between each group,

a convolution with stride 2 is used to downsample the spatial dimensions. Finally, global-average pooling is applied before a fully connected readout layer.

Dataset composition. We constructed thirteen datasets from subsets of CIFAR-10. The thirteen training sets ranged in size from 10 to 40960, and consisted of between 2^0 and 2^{12} examples per class. In addition, we constructed a validation set of 5000 images taken from the CIFAR-10 training set which we used for early stopping. Finally, we use the standard CIFAR-10 test set to report performance.

Whitening. We performed ZCA whitening using only the training examples to compute the whitening transform.

Training and Measurements. We used a cross entropy loss. We performed full-batch gradient descent training with a learning rate of 10^{-3} until the training error was less than 10^{-3} . We use TPUV2 accelerators for these experiments and assign one image class to each chip. Care must be taken to aggregate batch normalization statistics across devices during training. After training, the test accuracy at the training step corresponding to the highest validation accuracy was reported. At each dataset size, this procedure was repeated twice, using two different random seeds. Means and standard errors across seeds were calculated and are plotted in Fig. 3(c).

E.4.2 CNN

Architecture. The network consisted of a single ResNet-50 convolutional block followed by a flattening operation and two fully connected layers of sizes 100 and 200, successively. Each dense layer had a \tanh nonlinearity and was followed by a layer norm operation.

Dataset composition. Training sets were of eleven sizes: 10, 20, 40, 80, 160, 320, 640, 1280, 2560, 5120, and 10240 examples. A validation set of 10000 images was split from the CIFAR-10 training set.

Training and Measurements. We used a cross entropy loss. Training was accomplished once with the Gauss-Newton method (see [46] for details), once with full batch gradient descent, and once with a regularized Gauss-Newton method. With a regularizer $\lambda \in [0, 1]$, the usual preconditioning matrix B of the Gauss-Newton update was modified as $((1 - \lambda)B + \lambda I)^{-1}$. This method interpolates between pure Gauss-Newton ($\lambda = 0$) and gradient descent ($\lambda = 1$). In the Gauss-Newton experiments, we used conjugate gradients to solve for update directions; the sum of residuals of the conjugate gradients solution was required to be at most 10^{-5} .

For the gradient descent and unregularized Gauss-Newton experiments, at each training set size, ten CNNs were trained beginning with seven different initial learning rates: $2^{-8}, 2^{-6}, 2^{-4}, 2^{-2}, 1, 4$, and 16. After the initial learning rate, backtracking line search was used to choose subsequent step sizes. Models were trained until they achieved 100% training accuracy. The model with the initial learning rate that achieved the best validation performance of the seven was then selected. Its test performance on the CIFAR-10 test set was evaluated at the training step corresponding to its best validation performance. The entire procedure was repeated for five random seeds. In Fig. 3(d), we have plotted average test and validation losses over the random seeds as functions of dataset size and training algorithm. In Fig. 4(c), we have plotted an example of the validation and training performance trajectories over the course of training for a training set of size 10240.

For the regularized Gauss-Newton experiment, the only difference is that we trained one CNN at each initial learning rate per random seed, and then selected the model with the best validation performance. In Fig. 5, we have plotted average metrics over the five random seeds. Errorbars and shaded regions indicate twice the standard error in the mean.